RSC Advances

ROYAL SOCIETY OF CHEMISTRY

www.rsc.org/advances

Ti powder-assisted synthesis of Ti^{3+} self-doped TiO_2 nanosheets with enhanced visible-light photoactivity

Jinghua Cai, Ze'ai Huang, Kangle Lv*, Jie Sun, Kejian Deng

Key Laboratory of Catalysis and Materials Science of the State Ethnic Affairs Commission & Ministry of Education, South-Central University for Nationalities, Wuhan 430074, P.R. China.

Tel: +86-27-67842752, Fax: +86-27-67842752

E-mail: lvkangle@mail.scuec.edu.cn (K.L. Lv)

Abstract

TiO_2 nanocrystals with exposed high-energy (001) facets have been reported to show higher photocatalytic activity than those with exposed traditional (001) facets. However, they can only be excited by UV light. In this paper, visible-light responsive Ti^{3+}-doped TiO_2 nanosheets with exposed (001) facets were one-pot fabricated by hydrothermal treatment of the mixture solution of tetrabutyl titanate (80 mmol) and hydrofluoric acid (80 mmol) in the presence of Ti powder (0-12 mmol) at 200 ^oC for 24 h. The prepared Ti^{3+}-doped TiO_2 nanosheets photocatalyst were characterized by X-ray diffraction (XRD), transmission electron microscopy (TEM), scanning electron microscopy (SEM), diffuse reflectance spectroscopy (DRS), Raman spectrum, X-ray photoelectron spectroscopy (XPS) and nitrogen adsorption–desorption isotherms. The photocatalytic activity was evaluated by a photoluminescence (PL) technique using coumarin as a probe molecule under visible-light irradiation. The experimental results show that visible-light photocatalytic activity of the prepared photocatalyst increase first and then decrease with increasing the amount of Ti powder. Ti^{3+}-TiO_2 nanosheets prepared in the presence of 4 mmol Ti powder shows the highest visible-light photoactivity.

Keywords: Titanium dioxide; Nanosheets; Visible-light photocatalytic activity; Hydroxyl radicals; Titanium powder.

1. Introduction

As a prototype photocatalyst, titanium dioxide (TiO_2) has received the greatest attention due to its strong photo oxidization power, cost effectiveness, and long term stability against photo- and chemical-corrosion[1]. However, the large band gap of pure TiO_2 (~3.2 eV) renders it only active in the ultraviolet (UV) region. Thus, only UV light (<5% of total solar energy) can be utilized to generate electron–hole pairs for the desired photoelectrochemical processes. Hence, much attention has been paid to improve the photocatalytic activity of TiO_2 photocatalyst[2-5].

The photocatalytic performance of TiO_2 is mainly dependent on its morphology, crystal structure, light absorption, and surface chemical environment[6-9]. In recent years, anatase TiO_2 nanocrystals with exposed (001) facets have been reported to show higher photocatalytic activity than those with exposed traditional (101) facets due to the higher energy of (001) facets[10-15]. Unfortunately, TiO_2 nanocrystals with exposed (001) facets still can only be excited under the irradiation of UV light. From the view of practical applications, it is of great importance to fabricate visible-light responsive high-energy TiO_2 nanocrystals[16-19].

Up to now, various approaches have been developed to extend its intrinsic absorption to visible-light range by modifying the band structure of TiO_2, such as doping with transition metals[20,21] or non-metals[2,22,23]. However, the doping, especially in the originally crystal growth process, of TiO_2 with dominant (001) facets to enhance light absorption in visible-light range is restricted by the critical crystal growth environment[19]. Although further element doping by heat treatment can extend the light absorption edge of TiO_2 to the visible range, the strategy is limited by the possibility of leakage of hazardous dopants into the environment, dopant-induced charge recombination and/or traps, and dopant-induced thermal instability[17].

Another method to improve the photocatalytic activity of TiO_2 with dominant (001) facets in visible region is by self-doping TiO_2 with Ti^{3+}. Till now, the methods for forming Ti^{3+} are variable such as vacuum, inert and reducing gas atmosphere heating[18,24,25]. However, these methods have a lot of limitations such as critical experiment environment, complication and highly cost[26,27]. For example, Xia *et al.* reported the fabrication of Ti^{3+}-doped TiO_2 nanocrystals by heat treatment of pristine TiO_2 sample under low vacuum (2-5 mtorr) at 150 ^oC for as long as 4 days[28]. Therefore, developing a simple method to synthesize Ti^{3+} self-doped TiO_2 is a very promising topic.

Herein, we report a simple method to fabricate visible-light responsive TiO_2 nanosheets with dominant (001) facets using Ti powder as reductant. The effects of Ti on morphology, texture structure and light-harvesting ability of TiO_2 nanosheets was studied.

2. Experimental section

2.1. Sample Preparation.

Ti^{3+}-doped TiO_2 nanosheets with exposed high-energy (001) facets were prepared by hydrothermal treatment the mixture solution of tetrabutyl titanate (TBT), hydrofluoric acid (HF) in the presence of Ti powder. Briefly, 4 ml (80 mmol) of HF solution (40 wt.%) were dropwise added into a Teflon beaker containing certain amount of titanium powder (0-12 mmol) under magnetic stirring. After Ti powder was completely dissolved, the obtained green solution was dropwise added into a Teflon beaker containing 80 mmol of TBT under continuous stirring. The resulted mixed solution was then transferred to a dried 100 mL Teflon-lined autoclave and kept at 200 ^oC for 24 h. After being cooled to room temperature, the precipitates were filtrated

through a membrane filter (pore size 0.45 μm) followed by thoroughly washed with 0.1 M NaOH to remove surface adsorbed fluoride ions, and rinsed with distilled water until the pH value of the filtrate is about 7. Then the precipitates were dried at room temperature. The resulted sample is denoted as Sx, where x represents the molar weight (in unit of mmol) of Ti powder used (Table 1).

2.2 Characterization. The X-ray diffraction (XRD) patterns obtained on a D8-advance X-ray diffractometer (German Bruker). The accelerated voltage and applied current were 15 kV and 20 mA, respectively. The morphology of TiO_2 powders was observed on a transmission electron microscope (TEM) (Tecnai G20, USA) using an acceleration voltage of 200 kV and a field emission scanning electron microscope (SEM) (S-4800, Hitachi, Japan) with an acceleration voltage of 10 kV, respectively. UV-Vis diffuse reflectance spectra were obtained on a UV-Vis spectrophotometer (LambdaBio35) using $BaSO_4$ as the reference. Raman spectra were recorded at room temperature using a laser confocal Invia Raman spectrometer (Renishaw, UK) in the backscattering geometry with a 514.5 nm Ar^+ laser as an excitation source. X-ray photoelectron spectroscopy (XPS) measurements were done with a Kratos XSAM800 XPS system with Mg Kαsource and a charge neutralizer, all the binding energies were referenced to the C1s peak at 284.8 eV of the surface adventitious carbon. Nitrogen adsorption–desorption isotherms were obtained on an ASAP 2020 (Micromeritic Instruments, USA) nitrogen adsorption apparatus. All the samples were degassed at 150 ^oC prior to Brunauer–Emmett–Teller (BET) measurements. The BET specific surface area (S_{BET}) was determined by a multipoint BET method using the adsorption data in the relative pressure P/P_0 range of 0.05–0.30. The desorption isotherm was used to determine the pore size distribution by using the Barret–Joyner–Halenda (BJH)

method. The nitrogen adsorption volume at P/P_0 = 0.994 was used to determine the pore volume and average pore size.

2.3 Measurement of the formation of hydroxyl radicals. The photocatalytic activity of the prepared TiO_2 nanosheets was evaluated by measurement the formation rate of hydroxyl radicals (·OH) in TiO_2 suspension under visible-light irradiation by a photoluminescence (PL) technique using coumarin as a probe molecule, which readily reacted with ·OH radicals to produce highly fluorescent product, 7-hydroxycoumarin[14]. Briefly, a 3 W LED lamp (UVEC-4 II, Shenzhen lamplic, China) emitted mainly at 420 nm is used as light source, which is placed outside a Pyrex-glass reactor at a fixed distance (ca. 5 cm). During the photocatalytic reaction, the reactor was mechanically stirred at a constant rate. The suspensions of TiO_2 (1.0 gL^{-1}) containing coumarin (0.5 $mmolL^{-1}$) is mixed under magnetic stirring, and then was shaken overnight. At given intervals of irradiation, small aliquots were withdrawn by a syringe, and filtered through a membrane (pore size 0.45 μm). The filtrate was then analyzed on a Hitachi F-7000 fluorescence spectrophotometer by the excitation with the wavelength of 332 nm. For comparison, the UV light photocatalytic activity of the sample was also evaluated under the irradiation of a 3W UV LED lamp with emitted mainly at 365 nm under other identical conditions.

3. Results and discussion

3.1. Phase structure and morphology.

The phase structure, crystallization and shape of TiO_2 are of great influence on its photocatalytic activity. Therefore, XRD was used to analyze the phase structures and crystallization of the prepared TiO_2 samples.

Fig. 1A shows the XRD patterns of the photocatalysts. It can be seen that all of the prepared samples appeared to be pure anatase TiO_2 (JCPDS no. 21-1272)[29]. Further

observation shows that the intensity of XRD peaks of anatase become steadily stronger and the width of XRD diffraction peaks of anatase becomes slightly narrower with increasing the amount of Ti powder, indicating the enhancement of crystallization. After addition of 12 mmol of Ti powder, the crystallization of TiO_2 was found to enhance almost 50% (Table 1). It was reported that the acidity of solution plays an important role on the crystallization of TiO_2[30]. The addition of Ti powder into HF solution can affect the acidity of HF, forming of Ti^{3+} and H_2 gas (Eq. 1). The observed gas bubbling and formation of dark blue solution after addition of Ti powder confirm the formation of Ti^{3+} and H_2 gas. The formed Ti^{3+} can therefore introduced into the crystal lattice of TiO_2 nanosheets with exposed (001) facets during hydrothermal reaction.

$$Ti + HF = TiF_3 + H_2\uparrow \quad (1)$$

Consistent with the report in literature[13,31,32], the prepared TiO_2 nanocrystals were sheet-like in structure (TEM and SEM images shown in Fig. 2). It is clear that all the photocatalysts have similar side length (60-80 nm) and thickness (5-6 nm) whatever the absence or presence of Ti powder. Inset of Fig. 1c shows the high resolution TEM image of a nanosheet for S4 sample, which was erected on copper grid. The lattice spacing of ca. 0.235 nm is corresponding to the {001} plane of anatase TiO_2, confirming the exposure of (001) facets[13,31].

3.2 UV–vis absorption.

It was found that after addition of Ti powder, the optical response of the photocatalyst in the visible light region changes from white to blue, which was characterized by the UV-vis absorption spectrum (Fig. 3). Compared with S0 sample (undoped TiO_2), the spectra of the Ti^{3+} self-doped TiO_2 samples (TiO_{2-x}) exhibit a strong broad absorption band between 400 and 800 nm, covering nearly the entire

visible range, and the absorption increases with increasing the amount of Ti powder due to the increased concentration of Ti^{3+} in lattice. The strong absorption in the visible-light region implies that the prepared samples can be activated by visible-light and that more photo-generated electron-hole pairs can be created to participate in the photocatalytic oxidation reactions[17].

3.3 Raman and XPS analysis.

It is well known that Raman spectroscopy, which is originated from the vibration of molecular bonds with high measuring sensitivity, is a simple, efficient, well-established technique and accurate alternative approach to study the signicant structural changes in titania[33]. Fig. 4 compares the Raman spectra of undoped (S0) and Ti^{3+} self-doped TiO_2 (S4). It can be seen that the intensity of all the diffraction peaks weakened after Ti^{3+} doping, demonstrating the increase in the number of oxygen vacancies in the lattice of Ti^{3+} self-doped TiO_2 nanosheets due to the introduction of Ti^{3+} into the lattice[18]. Oxygen deficiency can transfer its extra two electrons to the adjacent two Ti^{4+} atoms to form Ti^{3+}, and the presence of the oxygen vacancies lead to the change of atomic coordination numbers and bonding length of the Ti-O-Ti network in Ti^{3+} self-doped TiO_2 nanosheets. Therefore, it is not strange to see that the intensities of Raman peaks decrease with increase in the Ti/TBT molar ratio. Liu *et al.*[34] found that the intensities of non-stoichiometric TiO_{2-x} Raman peaks can be recovered by the removal of oxygen deficiency after calcination in air, further confirmed that it is the formation of Ti^{3+} due to oxygen vacancies that results in the weaken of Raman peaks. The Raman peak broadening effect in non-stoichiometric TiO_{2-x} nanoparticles was also observed by Zhu *et al.*, which was also attributed to the presence of lattice disorder as a result of oxygen vacancies[33].

Fig. 5A compares the XPS survey spectra of the prepared TiO_2 powders, which shows that all of the samples contain Ti, O, and F elements and a trace amount of C. The C element is ascribed to the residual carbon from precursor solution and the adventitious hydrocarbon from the XPS instrument itself[35]. Fig. 5B shows typical Ti 2p core level XPS spectrum of Ti^{3+} self-doped TiO_2 (S4). The Ti 2p peaks of Ti^{3+} self-doped TiO_2 can be de-convoluted into four peaks as Ti^{3+} 2p3/2 at 457.9 eV, Ti^{4+} 2p3/2 at 458.8 eV, Ti^{3+} 2p1/2 at 463.8 eV and Ti^{4+} 2p1/2 at 464.5 eV[16,18]. The presence of Ti^{3+} species on the surface or in the bulk can suppress the recombination of electron–hole pairs, and therefore promote the photocatalytic activity.

3.4 Nitrogen sorption.

Fig. 6 shows nitrogen adsorption–desorption isotherms and the corresponding pore size distribution curves of undoped (S0) and Ti^{3+} self-doped TiO_2 nanosheets (S4). It can be seen that both of the two samples displayed type IV nitrogen isotherm with a hysteresis loop at relative pressure range of 0.7-1.0 (H3), suggesting narrow slit-shaped pores that are generally associated with plate-like particles, which agrees well with their sheet-like morphology (Fig. 2)[14].

Table 1 summarizes the physical properties of the photocatalysts. It can be seen that all the prepared TiO_2 samples have similar BET specific surface areas (80-90 m^2g^{-1}) and pore structures. Note that the average pore sizes of TiO_2 nanosheets were less than the average side length. This is due to the fact that these nanosheets are not individually dispersed and easily connected with each other along [001] direction to minimize the surface energy (Fig. 2). Therefore, the enhanced photocatalytic activity of Ti^{3+}-doped TiO_2 nanosheets should result from enhanced light-harvesting ability instead of the change from surface areas and pore structures.

3.5 Photocatalytic activity.

It was reported that several non- or weakly luminescent molecules, such as terephthalic acid and coumarin, produce strongly luminescent compounds with •OH radical[7,36]. •OH radicals formed in visible-illuminated TiO_2 suspensions were thought to be the main oxidative species which are responsible for the degradation of organic pollutant. Therefore, the formation rate of •OH radicals in solution was used to compare the relative photocatalytic activity of TiO_2. Here coumarin is used as a probe to evaluate the visible-light photocatalytic activity of the Ti^{3+} self-doped TiO_2 nanosheets, which readily reacted with ·OH radicals to produce highly fluorescent product, 7-hydroxycoumarin[8].

Inset of Fig. 7A shows the typical PL spectral changes observed during illumination of the suspensions of Ti^{3+}-doped TiO_2 nanosheets. It is observed that the PL intensity of photo-generated 7-hydroxycoumarin at 450 nm (excited at 332 nm) increases with irradiation time, obeying a pseudo-zero order reaction rate equation in kinetics. Fig. 7A records the time course of the PL intensity of 7-hydroxycoumarin at 450 nm during the irradiation of the photocatalyst. It is clearly seen that the PL intensity at 450 nm increases linearly against the irradiation time, reflecting the stability of the photocatalyst. It was reported in literature that surface adsorbed Ti^{3+} is unstable, which can easily be oxidized[36]. Therefore, a conclusion can be drawn from our work that the Ti^{3+} was doped into the lattice of TiO_2 nanosheets instead of on the surface. The slope for the curve of PL intensity versus illumination time (rate constant), which represents the photocatalytic activity of the photocatalyst, increases first and then decreases with increasing the amount of Ti powder. Ti^{3+} self-doped TiO_2 nanosheets prepared in the presence of 4 mmol Ti powder shows the highest photocatalytic activity with a rate constant of 4.84, which is 2.67 and 2.51 times higher than undoped S0 sample (rate constant 1.82) and Degussa P25 TiO_2 (rate

constant 1.93), respectively.

For comparison, the photocatalytic activity of the photocatalyst was also evaluated under UV irradiation (Fig. 8). The photocatalytic activity of S4 (rate constant of 44.8) was found to be 1.54 and 1.13 times higher than that of undoped S0 (rate constant of 29.0) and P25 TiO_2 (rate constant of 39.6), respectively. The experimental results reflect that the enhanced visible-light photocatalytic activity of Ti^{3+} self-doped TiO_2 nanosheets is not based on the sacrifice of their UV light activity.

Why Ti^{3+}-doped TiO_2 nanosheets show high visible photocatalytic activity? This is due to the formation of Ti^{3+} dopant levels which are below the conduction band of TiO_2 (Fig. 9). It is the formed dopant levels that result in the visible-light photocatalytic activity of Ti^{3+} self-doped TiO_2 nanosheets[35]. However, high concentrated Ti^{3+} will result in the formation of recombination center for photo-generated electron-hole pairs, which is harmful for the photocatalytic activity of TiO_2.

4. Conclusions.

In summary, we developed a facile Ti-assisted hydrothermal method for preparation of Ti^{3+} self-doped TiO_2 nanosheets with dominant (001) facets. Owing to the formation of dopant levels below the conduction band of TiO_2, the photocatalyst showed improved light-harvesting ability in visible-light region and enhanced the visible-light photocatalytic activity. However, high-concentrated Ti^{3+} dopant is harmful for the photocatalytic activity of TiO_2 nanosheets due to the formation of recombination centers for photo-generated electron-hole pairs. The enhanced visible-light photocatalytic activity of Ti^{3+} self-doped TiO_2 nanosheets is not based on the sacrifice of their UV light activity. This work opens a new strategy for the design

of advanced visible-light photocatalyst.

Acknowledgements

This work was supported by Program for New Century Excellent Talents in University (NCET-12-0668) and National Natural Science Foundation of China (21373275 & 20977114).

References:

[1] X.B. Chen and S.S. Mao, *Chem. Rev.*, 2007, **107,** 2891.

[2] G. Liu, H.G. Yang, X.W. Wang, L. Cheng, J. Pan, G.Q. Lu and H.M. Cheng, *J. Am. Chem. Soc.*, 2009, **131,** 12868.

[3] J.G. Yu, G.P. Dai, Q.J. Xiang and M. Jaroniec, *J. Mater. Chem.*, 2011, **21,** 1049.

[4] Y. Liu, L.F. Chen, J.C. Hu, J.L. Li, and R. Richards, *J. Phys. Chem. C*, 2010, **114,** 1641.

[5] J. Sun, X. Yan, K.L. Lv, S. Sun, K.J. Deng and D.Y. Du, *J. Mol. Catal. A*, 2013, **367,** 31.

[6] S.W. Liu, J.G. Yu and M. Jaroniec, *J. Am. Chem. Soc.*, 2010, **132,** 11914.

[7] K.L. Lv, J.G. Yu, K.J. Deng, X.H. Li and M. Li, *J. Phys. Chem. Solid*, 2010, **71,** 519.

[8] Z.A. Huang, Z.Y. Wang, K.L. Lv, Y. Zheng and K.J. Deng, *ACS Appl. Mater. Interfaces*, 2013, **5,** 8663.

[9] K.L. Lv, B. Cheng, J.G. Yu and G. Liu, *Phys. Chem. Chem. Phys.*, 2012, **14,** 5349.

[10] H.G. Yang, C.H. Sun, S.Z. Qiao, J. Zou, G. Liu, S.C. Smith, H.M. Cheng and G.Q. Lu, *Nature*, 2008, **453,** 638.

[11] J.S. Chen, Y.L. Tan, C.M. Li, Y.L. Cheah, D. Luan, S. Madhavi, F. Boey, L.A.

Archer and X.W. Lou, *J. Am. Chem. Soc.*, 2010, **132,** 6124.

[12] B.H. Wu, C.Y. Guo, N.F. Zheng, Z.X. Xie and G.D. Stucky, *J. Am. Chem. Soc.*, 2008, **130,** 17563.

[13] Y. Zheng, K.L. Lv, Z.Y. Wang, K.J. Deng and M. Li, *J. Mol. Catal. A*, 2012, **356,** 137.

[14] Z.Y. Wang, K.L. Lv, G.H. Wang, K.J. Deng and D.G. Tang, *Appl. Catal. B*, 2010, **100,** 378.

[15] K.L. Lv, Q.J. Xiang and J.G. Yu, *Appl. Catal. B*, 2011, **104,** 275.

[16] L. Pan, J.J. Zou, S.B. Wang, Z.F. Huang, A. Yu, L. Wang and X.W. Zhang, *Chem. Commun.*, 2013, **49,** 6593.

[17] X. Liu, S.M. Gao, H. Xu, Z.Z. Lou, W.J. Wang, B.B. Huang and Y. Dai, *Nanoscale*, 2013, **5,** 1870.

[18] W. Wang, Y.R. Ni, C.H. Lu and Z.Z. Xu, *RSC Adv.*, 2012, **2,** 8286.

[19] W. Wang, C.H. Lu, Y.R. Ni, J.B. Song, M.X. Su and Z.Z. Xu, *Catal. Commun.*, 2012, **22,** 19.

[20] H.S. Zuo, J. Sun, K.J. Deng, R. Su, F.Y. Wei and D.Y. Wang, *Chem. Eng. Technol.*, 2007, **30,** 577.

[21] K.L. Lv, H.S. Zuo, J. Sun, K.J. Deng, S.C. Liu, X.F. Li and D.Y. Wang, *J. Hazard. Mater.*, 2009, **161,** 396.

[22] M.H. Zhou and J.G. Yu, *J. Hazard. Mater.*, 2008, **152,** 1229.

[23] K.L. Lv, J.C. Hu, X.H. Li and M. Li, *J. Mol. Catal. A*, 2012, **356,** 78.

[24] Z.K. Zheng, B.B. Huang, J.B. Lu, Z.Y. Wang, X.Y. Qin, X.Y. Zhang, Y. Dai and M.H. Whangbo, *Chem. Commun.*, 2012, **48,** 5733.

[25] M.Y. Xing, J.L. Zhang, F. Chen and B.Z. Tian, *Chem. Commun.*, 2011, **47,** 4947.

[26] L.R. Grabstanowicz, S.M. Gao, T. Li, R.M. Rickard, T. Rajh, D.J. Liu and Tao.

Xu, *Inorg. Chem.*, 2013, **52,** 3884.

[27] W. Wang, C.H. Lu, Y.R. Ni and Z.Z. Xu, *CrystEngComm*, 2013, **15,** 2537.

[28] T. Xia , W. Zhang , J.B. Murowchick, G. Liu and X.B. Chen, *Adv. Engergy Mater.*, 2013, **3,** 1516.

[29] J.G. Yu, S.W. Liu and H.G. Yu, *J. Catal.*, 2007, **249,** 59.

[30] H.M. Zhang, Y. Wang, P.R. Liu, Y.H. Han, X.D. Yao, J. Zou, H.M. Cheng and H.J. Zhao, *ACS Appl. Mater. Interfaces*, 2011, **3,** 2472.

[31] X.G. Han, Q. Kuang, M.S. Jin, Z.X. Xie and L.S. Zheng, *J. Am. Chem. Soc.*, 2009, **131,** 3152.

[32] J.G. Yu, L.F. Qi and M. Jaroniec, *J. Phys. Chem. C*, 2010, **114,** 13118.

[33] Q. Zhu, Y. Peng, L. Lin, C.M. Fan, G.Q. Gao, R.X. Wang and A.W. Xu, *J. Mater. Chem. A*, 2014, **2**, 4429.

[34] G. Liu, H.G. Yang, X.W. Wang, L.N. Cheng, H.F. Lu, L.Z. Wang, G.Q. Lu and H.M. Cheng, *J. Phys. Chem. C*, 2009, **113,** 21784.

[35] J.C. Yu, J.G. Yu, W.K. Ho, Z.T. Jiang and L.Z. Zhang, *Chem. Mater.*, 2002, **14,** 3808.

[36] Z.K. Zheng, B.B. Huang, X.D. Meng, J.P. Wang, S.Y. Wang, Z.Z. Lou, Z.Y. Wang, X.Y. Qin, X.Y. Zhang and Y. Dai, *Chem. Commun.*, 2013, **49,** 868.

Table 1. Starting materials of the samples

sample	starting materials			characterization results			
	TBT (mmol)	HF (mmol)	Ti (mmol)	Crystallinity[a]	BET (m^2g^{-1})	PV (cm^3g^{-1})	APS (nm)
S0	80	80	0	1.00	88	0.25	11.4
S2	80	80	2.0	1.05	87	0.21	9.8
S4	80	80	4.0	1.18	81	0.19	9.6
S8	80	80	8.0	1.21	86	0.24	11.6
S12	80	80	12.0	1.46	80	0.21	12.1

[a]The relative crystallinity is evaluated via the relative intensity of anatase (101) plane diffraction peak using S0 sample as reference.

Figure captions

Fig. 1. XRD patterns of the prepared TiO_2 samples.

Fig. 2. TEM(a-e) and SEM (f) images of the prepared S0(a), S2(b), S4(c and f), S8(d) and S12(e) TiO_2 samples,respectively.

Fig. 3. UV-vis absorption spectra of TiO_2 photocatalysts prepared in the presence of different amount Ti powder. Inset showing the digital images of undoped (S0) and Ti^{3+}-self doped TiO_2 sample (S4), respectively.

Fig. 4. Raman spectra of S0 and S4, respectively.

Fig. 5. XPS survey spectra for the prepared TiO_2 nanosheets (A) and the high-resolution XPS spectrum of Ti 2p (B) for S4 sample.

Fig. 6. Nitrogen sorption–desorption isotherms and the corresponding pore size distributions (inset) of S0 and S4 photocatalyst, respectively.

Fig. 7. Time dependence of the induced photoluminescence intensity @ 450 nm (A) and the corresponding rate constants (B) under visible light irradiation. Inset of (A) recording the PL spectral changes observed during illumination of S4 photocatalyst.

Fig. 8. Time dependence of the induced photoluminescence intensity @ 450 nm under UV light irradiation.

Fig. 9. Schematic diagram for the visible-light responsive Ti^{3+}-doped TiO_2.

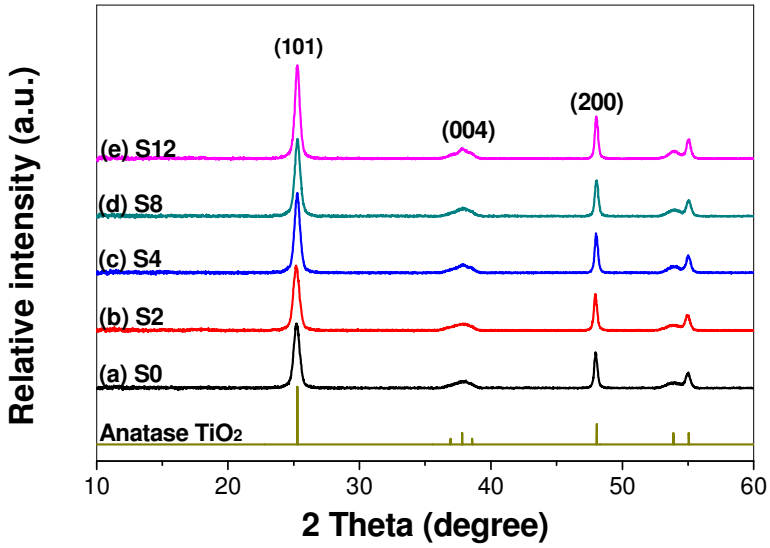

Fig. 1. XRD patterns of the prepared TiO_2 samples.

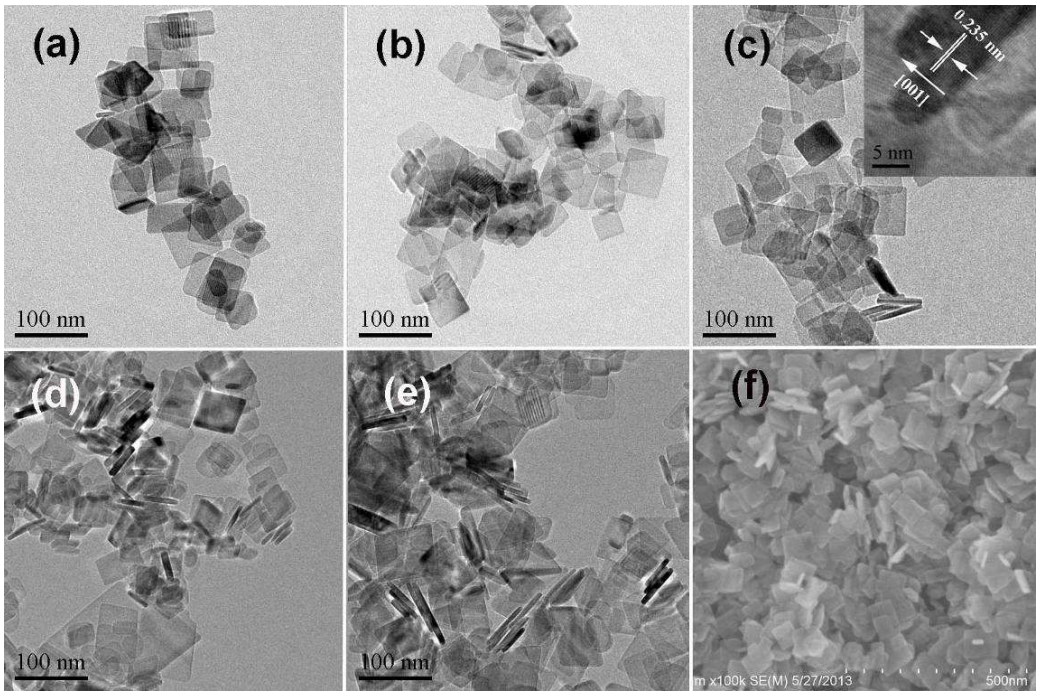

Fig. 2. TEM(a-e) and SEM (f) images of the prepared S0(a), S2(b), S4(c and f), S8(d) and S12(e) TiO_2 samples,respectively.

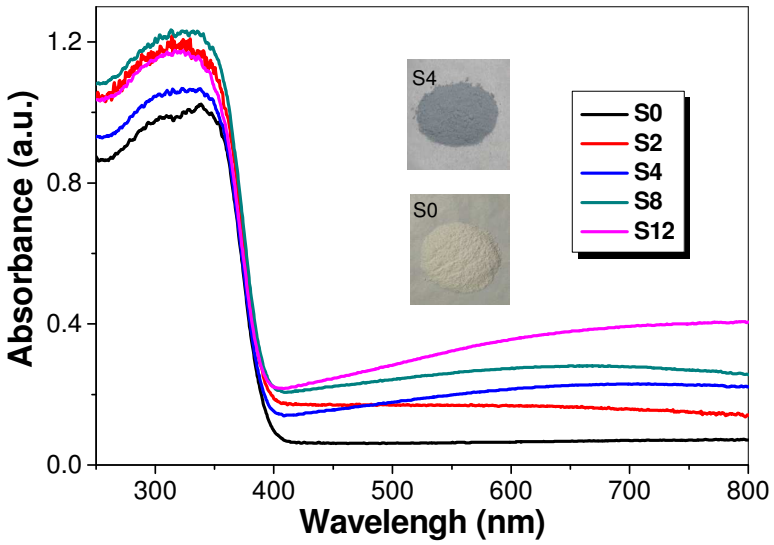

Fig. 3. UV-vis absorption spectra of TiO_2 photocatalysts prepared in the presence of different amount Ti powder. Inset showing the digital images of undoped (S0) and Ti^{3+}-self doped TiO_2 sample (S4), respectively.

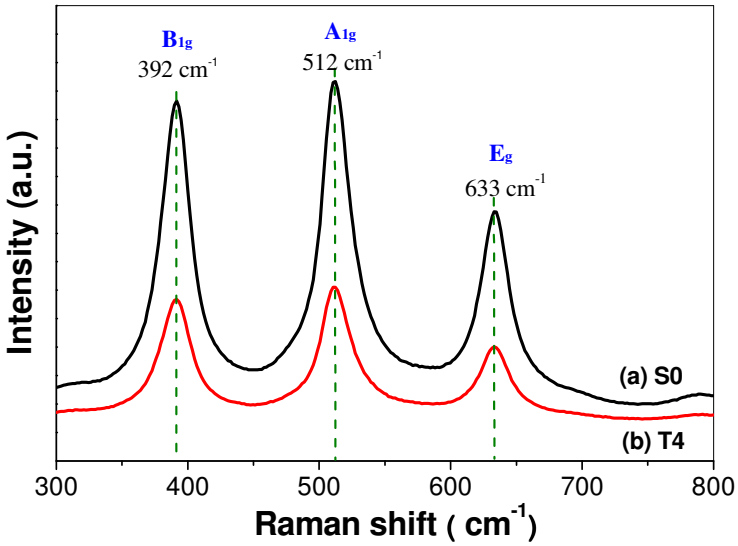

Fig. 4. Raman spectra of S0 and S4, respectively.

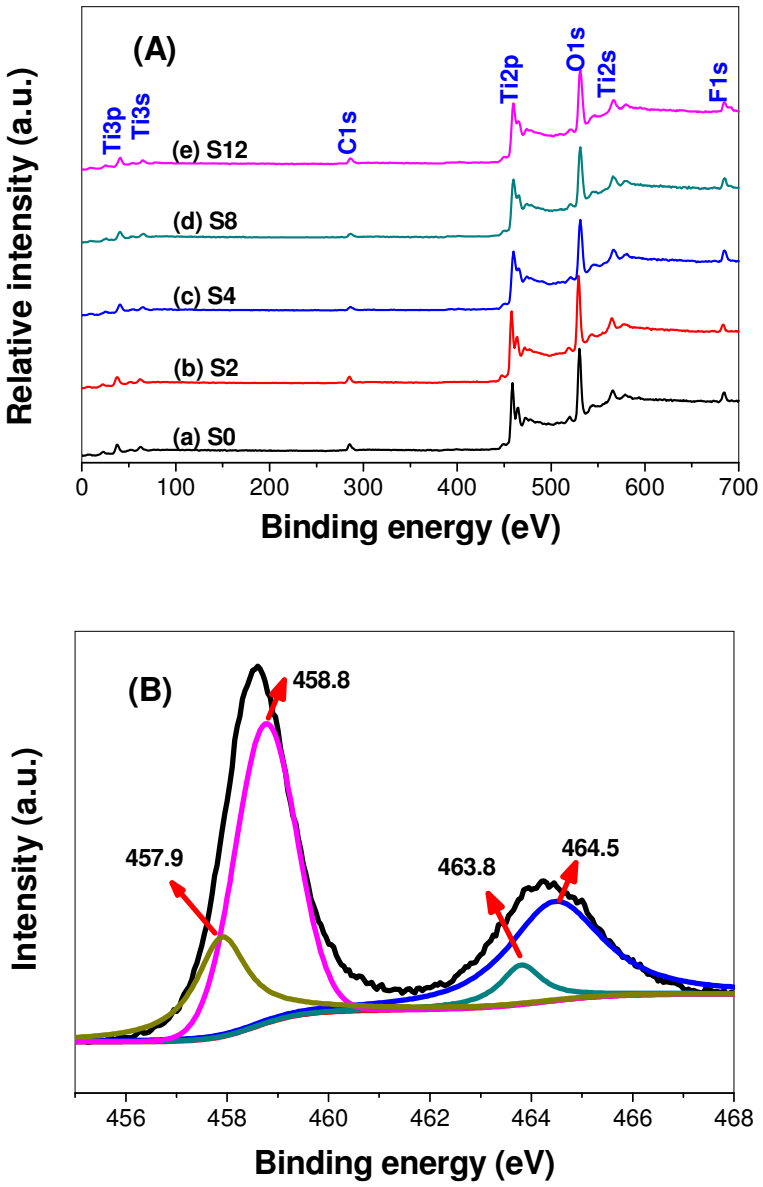

Fig. 5. XPS survey spectra for the prepared TiO_2 nanosheets (A) and the high-resolution XPS spectrum of Ti 2p (B) for S4 sample.

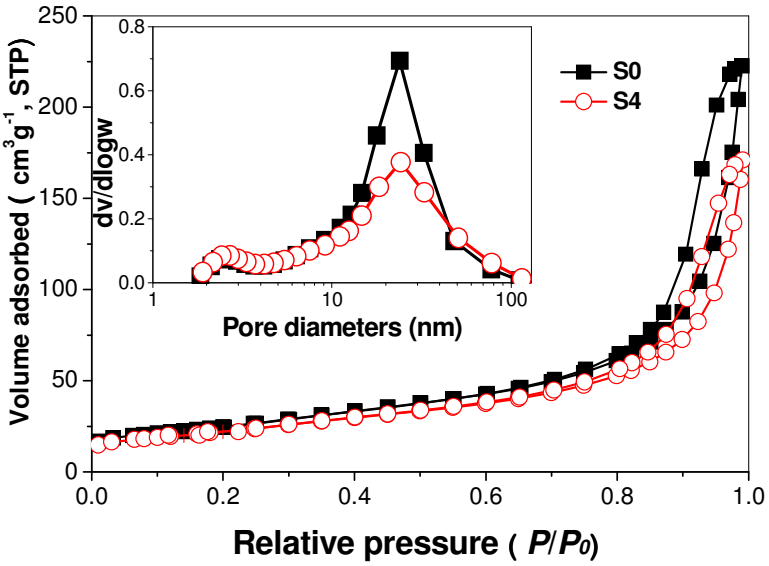

Fig. 6. Nitrogen sorption–desorption isotherms and the corresponding pore size distributions (inset) of S0 and S4 photocatalyst, respectively.

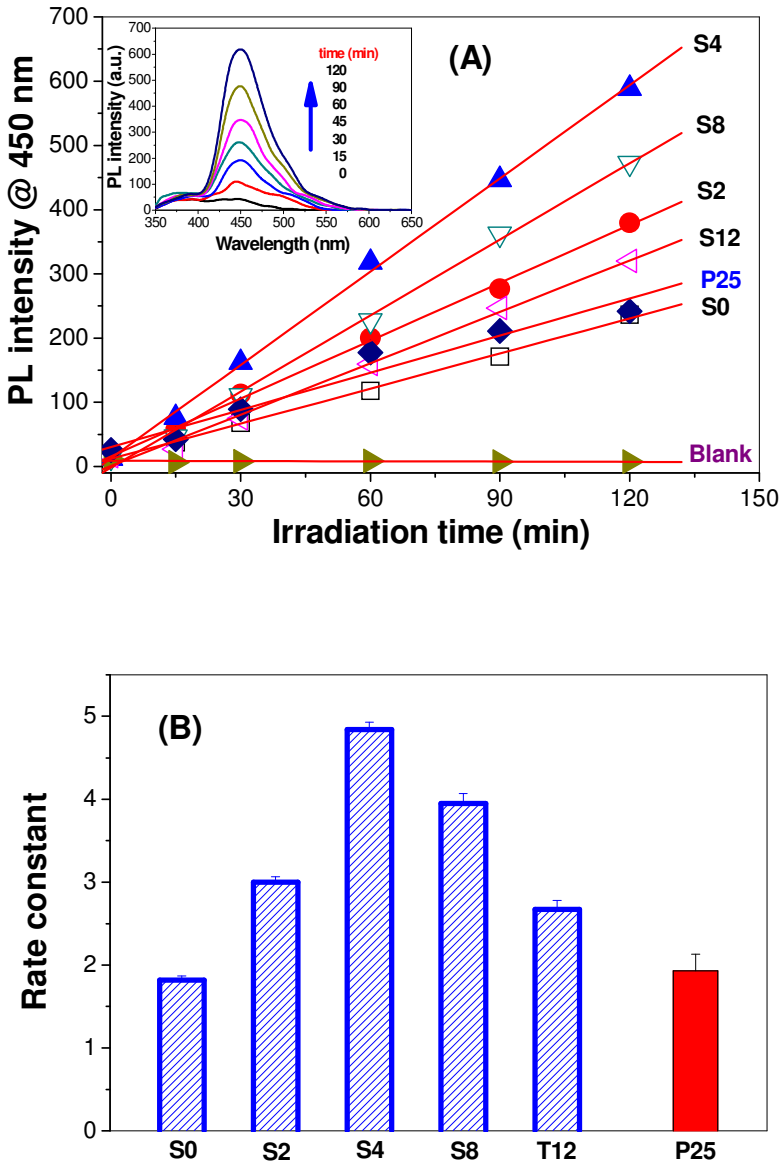

Fig. 7. Time dependence of the induced photoluminescence intensity @ 450 nm (A) and the corresponding rate constants (B) under visible light irradiation. Inset of (A) recording the PL spectral changes observed during illumination of S4 photocatalyst.

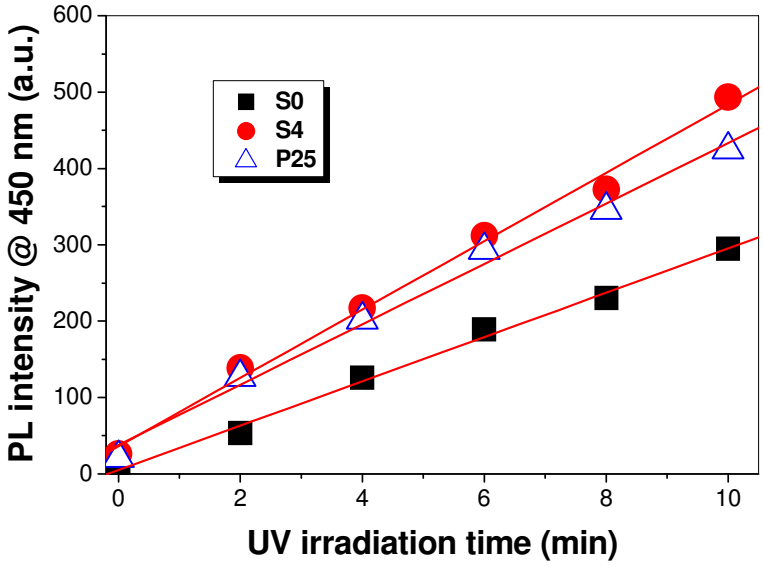

Fig. 8. Time dependence of the induced photoluminescence intensity @ 450 nm under UV light irradiation.

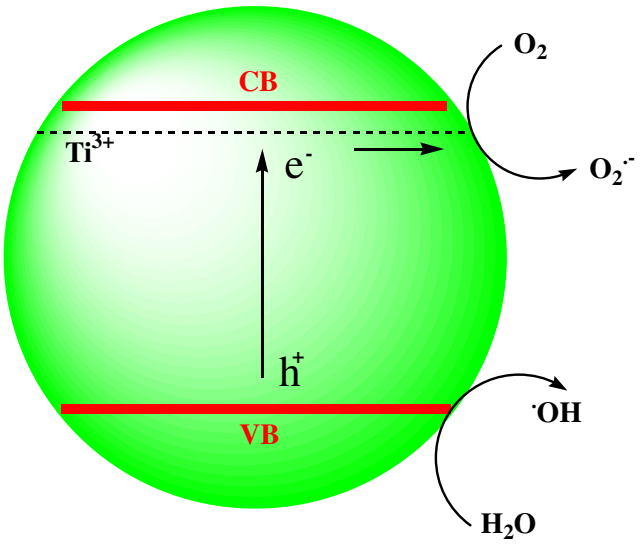

Fig. 9. Schematic diagram for the visible-light responsive Ti^{3+}-doped TiO_2.